



Recent progress on 2D ferroelectric and multiferroic materials, challenges, and opportunity

Banarji Behera¹ · Bijuni Charan Sutar² · Nihar Ranjan Pradhan³

Received: 25 January 2021 / Accepted: 16 April 2021
© Qatar University and Springer Nature Switzerland AG 2021

Abstract

Recently, the developments of two-dimensional (2D) ferroelectrics and multiferroics have attracted much more attention among researchers. These materials are useful for high-density devices for multifunctional applications such as sensors, transducers, actuators, non-volatile memories, photovoltaic, and FETs. Although several theoretical works have been reported on layered ferroelectrics, experimental work is still lacking in single to few-atomic layers of 2D ferroelectric materials. In this review, we have discussed the recent theoretical as well as experimental progress of 2D ferroelectric and multiferroic materials. The emphasis is given to the development of single to few-atomic layers of 2D ferroelectric materials. In this regard, the recent developments of 2D ferroelectric polarization on vanadium oxyhalides VOX_2 ($X=I, Br, Cl, \text{ and } F$), distorted phase $d1\text{-MoTe}_2$, In_2Se_3 , and $SnSe$ are discussed. $d1\text{-MoTe}_2$ shows Curie temperature (T_C) above room temperature, while few-layered In_2Se_3 shows in-plane ferroelectricity and interesting domain wall dynamics in a single atomic layer of $SnSe$. This follows the discussion of multiferroic materials based on transition metal oxyiodide MOI_2 ($M=Ti, V, \text{ and } Cr$), double perovskite bilayer, and iron-doped In_2Se_3 . While pristine In_2Se_3 shows ferroelectric properties, iron-doped In_2Se_3 shows multiferroicity. Finally, the potential applications of 2D ferroelectrics and multiferroics have been discussed that follow the challenges and opportunities in this field, which can guide the research community to develop next-generation 2D ferroelectric and multiferroic materials with interesting properties.

Keywords 2D materials · 2D dielectrics · 2D ferroelectrics · 2D multiferroics, Piezoelectric force microscopy

1 Introduction

A dielectric material is referred to an electrical insulator that can be polarized by an applied electric field. As these materials are insulators for electrical conduction, charge does not flow through them like in a conductor but the charges are shifted a small distance apart from their equilibrium position

along the direction of the applied electric field causing the materials to polarize, called dielectric polarization. Due to these basic properties, the dielectric materials have tremendous applications in energy storage, battery, capacitor, resonator, industrial coating, and many thin film applications like micro- and nanoelectronics as well as it helps to study the basic fundamental science in many materials. On the other hand, ferroelectric materials possess spontaneous electric polarization that can be reversed by the application of an external electric field [1, 2]. Due to the spontaneous polarization and analog to the spontaneous magnetization in ferromagnetic materials which was discovered before the discovery of ferroelectricity, the prefix “Ferro” was named in ferroelectric. Ferroelectric materials may not contain iron but “Ferro” refers to the spontaneous polarization. In addition to the dielectric and ferroelectric, some of the materials which exhibit two or more ferroic orders, i.e., ferroelectricity, ferromagnetism, ferroelasticity, or ferrotoroidicity in a single phase, are known as multiferroics [3–6] and the term “multiferroic” was first coined by Schmid in 1994 [3]. For multiferroic behavior,

✉ Banarji Behera
bbanarji@suniv.ac.in

✉ Nihar Ranjan Pradhan
nihar.r.pradhan@jsums.edu

¹ School of Physics, Sambalpur University, Jyoti Vihar, Burla, Sambalpur, Odisha 768 019, India

² Department of Physics, KMBB College of Engineering & Technology, Khurda, Odisha 752056, India

³ Layered Materials and Device Physics Laboratory, Department of Chemistry, Physics and Atmospheric Science, Jackson State University, Jackson 39217, MS, USA

materials with simultaneous presence of empty d shell (for ferroelectricity) and partially filled d or f shell (for ferromagnetism) are required. The mechanism of ferroelectricity and ferromagnetism is known as d^0 vs. d^n problem [7]. Technologically, the multiferroic materials play an important role in the next generation of intelligent devices, smart homes, autonomous devices, robotics, etc.

Nowadays, the development and design of 2D materials have received great attention among researchers for potential application in nanoelectronic devices. 2D materials such as MoS₂, MoSe₂, WSe₂, WS₂, MoTe₂, InSe, In₂Se₃, CuInSe, GaSe, *h*-BN, and black phosphorus (bP) have distinct chemical and physical properties including layered structure, high-surface area, layer-dependent tunable optical band gap, and variation of chemical compositions [8–17]. 2D Van der Waals (vdW) ferroelectric materials with non-centrosymmetric geometry show potential application in electronic devices and nanoelectromechanical systems. The tunable nature of polarization in ferroelectric materials by external applied electric fields and semiconducting nature with sizable band gap opens plenty of applications such as field-effect transistors, sensors and photonic devices, random access memory, and solar cells [18–23]. Earlier, it was thought that ferroelectricity may be possible up to certain critical thickness of the thin film but after development of microelectronics and thin film technology, particularly layered materials, several ferroelectric materials are reported in single to few-atomic layers which make them suitable candidates for miniaturization of the devices [24, 25]. The nanosheets made of 2D oxide may be the good solution in the era of 2D dielectrics [26]. Large variety of nanosheets has been synthesized by dividing layered oxides into single sheets [27–30]. The synthesized oxide nanosheets are from transition metal oxides consisting of d^0 cations (Ti⁺⁴, Nb⁺⁵, Ta⁺⁵, and W⁺⁶). These nanosheets can be used as high k -dielectrics due to their wide band gap semiconductors or insulator properties. However, more 2D materials have been prepared which includes 2D metallic materials [31], transition metal dichalcogenides [32], 2D metallic tungsten [33], 2D polymers [34], and 2D perovskites [35, 36]. Till now, more than 1000 2D materials have been predicted which are stable, although many of them are to be synthesized. Among these layered materials, several of them are dielectrics [37] and ferroelectric materials [38]. Similarly, a number of 2D multiferroic materials have been reported [39]. Recently, 2D ferromagnetic and ferroelectric materials have been reviewed for multifunctional applications [40–42]. Recently, ferroelectricity has been discovered in a moiré heterostructure system using a Bernal-stacked bilayer graphene (BLG) and hexagonal boron nitride (BN). Zheng et al. [43] demonstrated the ferroelectricity experimentally from the heterostructure stacking of BLG sandwiched between top and bottom layers of BN to form moiré patterns. In this moiré superlattice heterostructure, the rotational alignment between the BLG

and the encapsulating BN flakes plays an important role in the observed ferroelectricity. Such rotational alignment was introduced by aligning the straight edges of the middle BLG flake and one of the (top or bottom) BN flakes. The other degree of freedom is the relative angle between the top and bottom BN flakes. In devices, the top and bottom BN flakes have a relative angle of about 30° and about 0°, showing dramatic hysteresis response to the external applied electric field. In the devices where the top and bottom BN flakes have a relative angle of about 20°, it shows that the hysteresis is relatively weaker. This was again confirmed by the polarization measurements. It is noted that a normal BLG device, randomly stacked and sandwiched with BNs, does not show ferroelectric behavior. Only in the specific moiré heterostructure of BLG/BN stacked device, interaction-induced interlayer charge transfer and moiré flat bands occur, which leads to this type of unconventional nature of ferroelectric properties. Thus, there is a quest for new phenomena and exotic fundamental properties in these 2D systems, which have many potential technological applications.

In this review article, we discussed some of the recent developments on ferroelectric and multiferroic properties based on 2D materials [44, 47, 52, 54, 60, 65, 68, 75]. The recent theoretically predicted intrinsic ferromagnetic ferroelectric properties of monolayer VOX₂ (X = halogen, Cl, Br, and I) is presented, where it's predicted that the VOF₂ shows the largest in-plane ferroelectric polarizations (332 pC/m) among VOX₂ compounds. The multiferroic properties of 2D transition metal oxyiodide (MOI₂; M=Ti, V, Cr) have been discussed and explain the coexistence of d -electron ferroelectricity and magnetism. Experimental observations of ferroelectric with $T_C >$ room temperature have been observed on single to few atomic layers of MoTe₂ crystal. Doping is one of the interesting techniques to alter the physical properties of the materials. We have discussed the reported coexistence phase of ferroelectricity as well as ferromagnetism in 2D In₂Se₃ compounds doped with Fe atoms with a dopant concentration of 3.22%. Having ferroelectric and ferromagnetic properties in a single compound provides extraordinary opportunities for multifunctional electronic devices. Similar to the transition metal dichalcogenides, we have also discussed the recent discovery of ferroelectricity on 2D monochalcogenide SnSe, which shows interesting domain walls (DW) dynamics in 2D planes. Using appropriate technique to apply voltage to the 2D crystal, one can create and annihilate the DWs in a single atomic layer of SnSe.

2 Ferroelectric effect on vanadium oxyhalides

Recently, two-dimensional materials, VOF₂ monolayer, i.e., in the family of VOX₂ (X: halogen) oxyhalides, have been predicted theoretically by You et al. [44], and the materials

possess intrinsic ferroelectric and ferromagnetic properties. Generally, the displacement of the V ion from the center of an octahedron breaks the inversion symmetry and produces a spontaneous polarization. Using density functional theory (DFT) calculation, the VOF_2 monolayer has the largest in-plane ferroelectric polarization (332 pC m^{-1}) as compared to other VOX_2 , i.e., VOI_2 , VOBr_2 , and VOCl_2 [Fig. 1a]. The process of polarization reversal can be chosen by changing the position of V ions. The maximum energy barrier of the ferroelectric phase of VOF_2 is 0.33 eV when the lattice parameter is fixed. In this situation, V ion is allowed to move during polarization keeping O and F fixed positions. Due to the constraints of motion of O and F, the switching field of the ferroelectric phase is higher.

The energy barrier was calculated again without constraint of lattice parameters a and b such that the O and F ions can rearrange themselves with V ions during the polarization. The energy barrier of the ferroelectric phase of VOF_2 is reduced to 0.15 eV by self-organizing the lattice parameters a and b during switching. This value (0.15 eV) is smaller than VOCl_2 [Fig. 1b] [44]. Figure 1c displays the heat capacity as a function of temperature suggesting a magnetic phase transition occurs at 15 K. Since the magnetism occurs due to the spin of an unpaired electron in the d orbital of V^{4+} ion, the four collinear magnetic orders, i.e., FM, AFM (I), AFM (II), and AFM (III) are taken to understand the magnetic ground state (Fig. 1d). It is predicted that the ferromagnetic (FM) order is

more stable than other antiferromagnetic (AFM) orders. It also found that the Dzyaloshinsky–Moriya interaction [45, 46] distorts the texture of the spin to a spiral instead of collinear ferromagnetic (FM). This interaction accompanies the ferroelectric (FE) distortion. The magnetic orders were further studied by rearranging the spin direction with respect to V ions at an angle 120° [Fig. 1e] to understand the magnetic orders. It is also seen that the VOF_2 ground state is in FM order. This theoretical prediction may suggest to design spin ordered based VOF_2 material for potential candidates for two-dimensional multiferroic materials magnetoelectric effect [43].

3 Layer dependence ferroelectric properties of two-dimensional 1d-MoTe₂

Researchers have also discovered experimentally 2D ferroelectric on MoTe_2 nanosheets exfoliated on Pt substrate (Pt/Ti/SiO₂/Si) [47] using laser process [48]. The optical microscopy image of MoTe_2 in Fig. 2a shows a single-atomic layer to 9 layers and confirmed by AFM measurements [49]. Raman spectra of 2H- MoTe_2 (hexagonal phase) (Fig. 2b (i)) have two principal Raman modes, i.e., one at 174 cm^{-1} and another at 235 cm^{-1} , but for 1d- MoTe_2 , there are extra Raman modes appearing between 100 and 150 cm^{-1} [Fig. 2b (iii)] confirmed that the synthesized MoTe_2 is a distorted 1T phase. Figure 2c displays the room

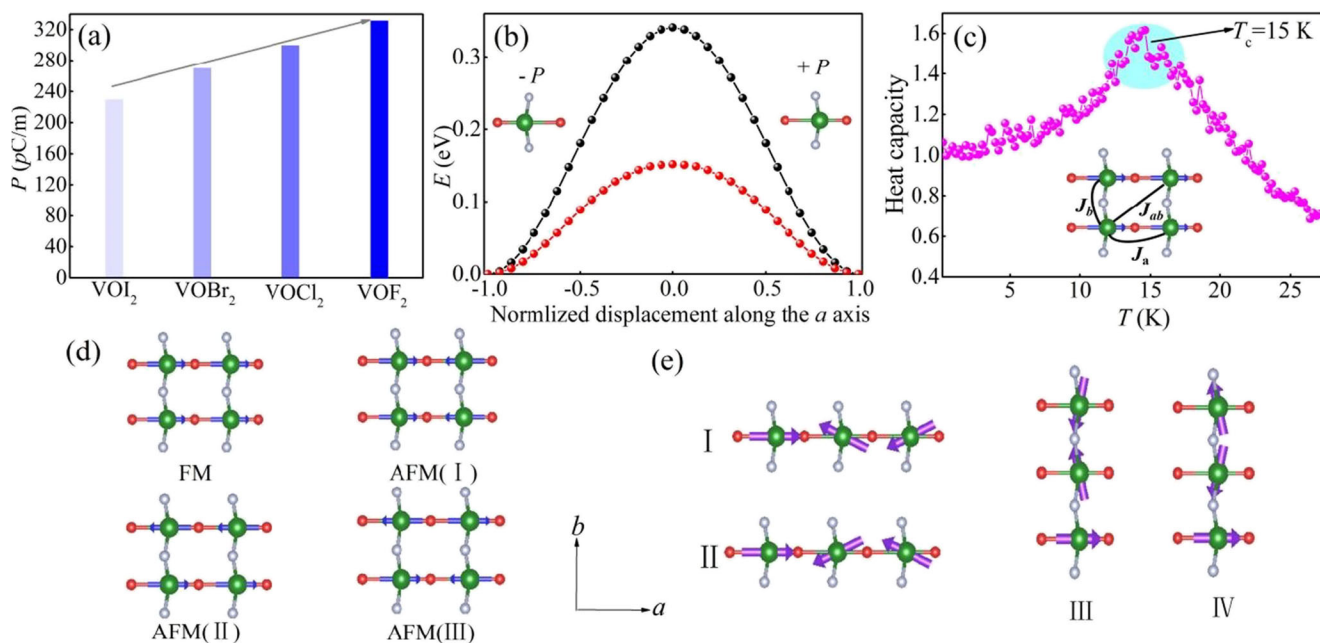


Fig. 1 **a** Calculated values of polarization of oxyhalides VOX_2 ($X=\text{I, Br, Cl, and F}$). **b** Energy barrier vs ferroelectric displacement during ferroelectric (FE) switching of vanadium (V) ions in VOF_2 . Black curve represents energy barriers where the lattice constants, i.e., a and b are unchanged and the red curves represent the same energy barrier with change in lattice constants during the switching. $+P$ and $-P$ denote the

polarization directions (insets) **c** Heat capacity vs temperature (T) of VOF_2 monolayer from Monte Carlo (MC) simulation and inset shows the exchange paths between V ions. **d** Four types of collinear magnetic orders, i.e., FM, AFM (I), AFM (II), and AFM (III). **e** Four types of 120° non-collinear magnetic orders. The figures are obtained with permission from Reference [44].

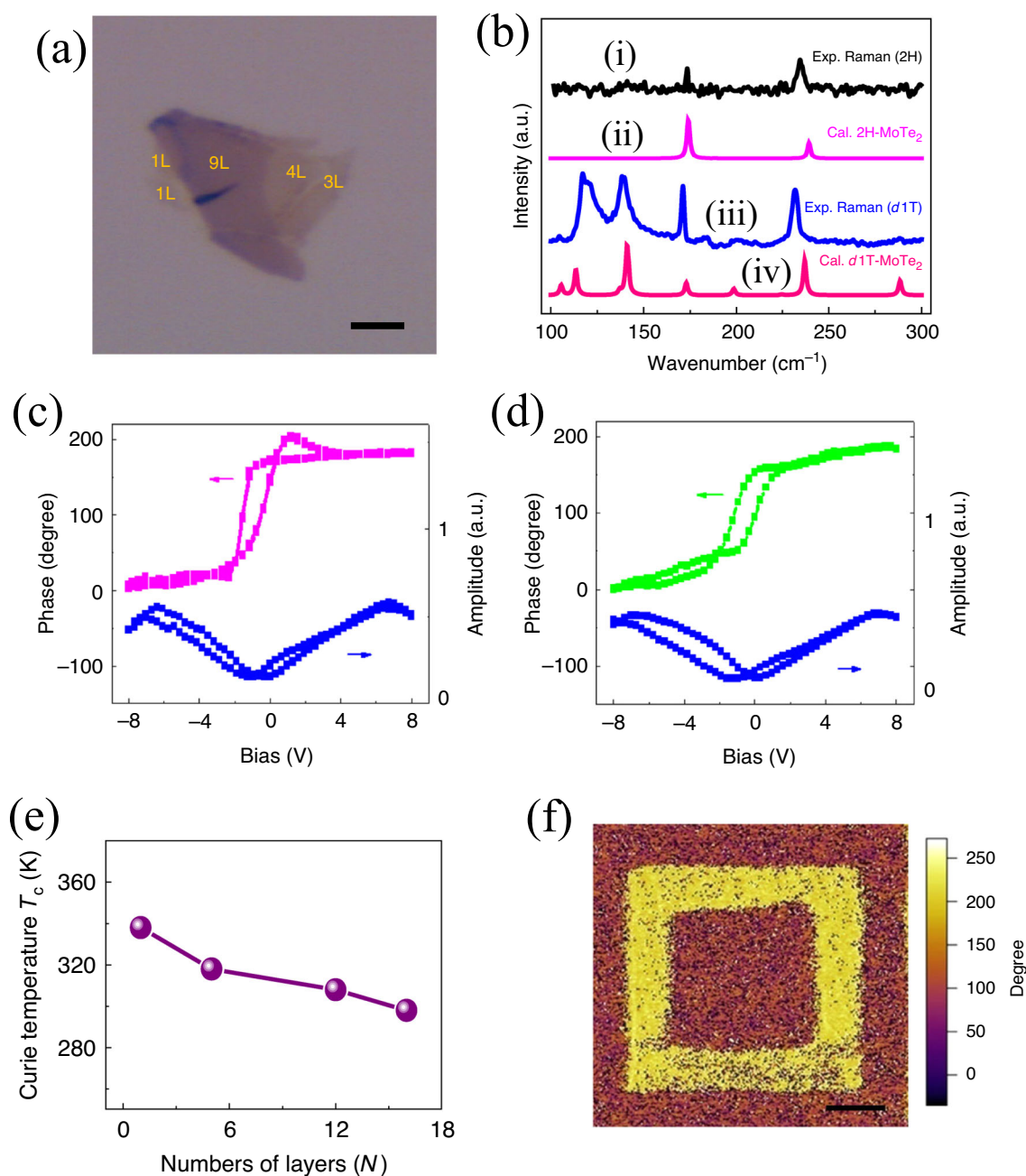


Fig. 2 Ferroelectricity on monolayer to few-atomic layers of distorted 1T-MoTe₂ crystal. **a** Optical microscope (OM) image of d1T-MoTe₂ on Pt substrate. Scale bar, 3 μm . **b** Raman spectra of 2H-MoTe₂ and d1T-MoTe₂. **c** and **d** PFM phase hysteresis and butterfly loops of monolayer and few layers d1T-MoTe₂ respectively. **e** Curie temperature of d1T-

MoTe₂ crystal as a function of number of layers. **f** PFM phase image of monolayer d1T-MoTe₂, where the electrical poling was applied by writing two square patterns with ± 8 V, scale bar, 1 μm . The figures are obtained with permission from Reference [47]

temperature Piezoresponse Force Microscopy (PFM) phase hysteresis, and butterfly loops of monolayer d1T-MoTe₂ exhibit the 180° phase difference between two out of plane polarization states and the amplitude minima of the loop confirms the ferroelectric behavior in the MoTe₂ nanosheets. The change in ferroelectric polarization behavior was studied in a few-layers d1T-MoTe₂ sample. Figure 2 d shows the PFM phase hysteresis behavior of a few-layered d1T-MoTe₂ and gives the perfect

switching of polarization behavior similar to the monolayer shown in Fig. 2c. The polarization on this few-layered sample was tested after 30 days and shows no change in polarization state. This indicates the stable ferroelectric behavior in monolayer or few atomic layers of d1T-MoTe₂. The Curie temperature (T_c) was measured as a function of the number of layers on d1T-MoTe₂ sample and presented in Fig. 2e, where T_c decreases with increasing number of layers. Interestingly, a single layer to few

atomic layers (~15 layers) shows that the T_C above room temperature makes d1T-MoTe₂ a promising candidate for the application of many ferroelectric based nanoscale electronic devices.

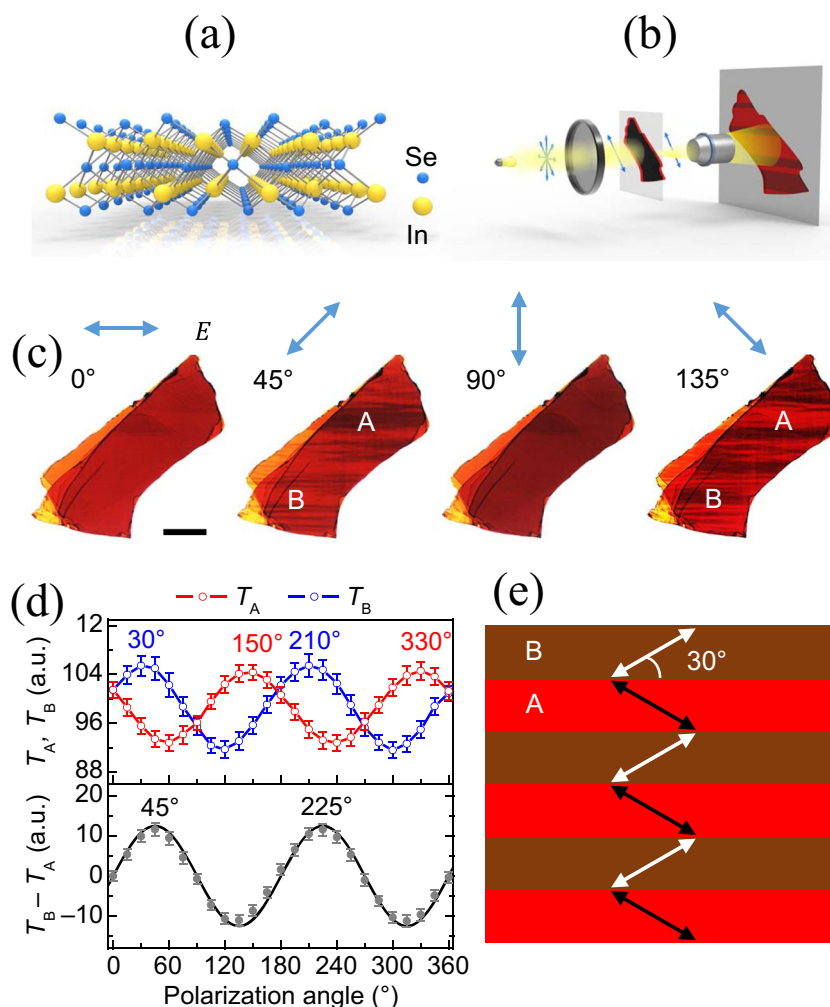
Further, the sample was studied for large scale polarization switching for practical applications using PFM phase imaging technique (Fig. 2f) by applying the voltage ± 8 V. The distinct phase contrast between the square pattern and rest of the sample reveals the switching of ferroelectric domains by applied electric field in a larger scale. It's very interesting to know that even though charge carrier mobility in monolayer of these 2D materials field-effect transistors suffers from the extrinsic effect from the substrate, defects, and moisture, ferroelectricity seems not to suffer from these effects [50, 51].

4 Room temperature in-plane ferroelectricity in Van der Waals In₂Se₃

As discussed above, ferroelectricity in layered vdW materials has potential applications for nonvolatile memory and low-power electronic, optoelectronic switches, etc. But to date, the ferroelectric layered materials in atomic scale are limited due to the difficulty in controlling the polarization vectors along the in-plane direction. Here, we have discussed the in-plane ferroelectricity on β -In₂Se₃ vdW layered material reported by Zheng et al. [52]. Here, the β -phase In₂Se₃ crystal was chosen, which has the rhombohedral structure and belongs to the R3m space group to elucidate the ferroelectric property. Figure 3 a shows the schematic of crystal structure indicates the five layers of basic building blocks of Se-In-Se-In-Se atoms across the plane (c-axis: perpendicular to the 2D plane). The a-b planes are on the 2D layer of the materials. The β -In₂Se₃ has threefold rotational symmetry about the c-axis can be seen easily from the Fig. 3 a. An experimental setup with polarization of light incident to the crystal plane is shown in the schematic of Fig. 3b for polarization-dependent optical measurements. Figure 3 c shows a sequence of optical images taken at room temperature of a 100-nm thick β -In₂Se₃ exfoliated crystal illuminated with various linear polarization angles on the plane of the crystal. The optical images are taken in transmission mode of the light signal as shown in the figure. Figure 3 c displays the series of optical images taken at different polarization angle of the light signal from a Nikon Eclipse optical microscope. The 0° polarization angle is defined as the light polarization direction along the horizontal direction (or perpendicular to the plane of the crystal or polarization is along the direction of propagation of light). There is no visible domain observed at 0° of light polarization, but interestingly, the optical image reveals the presence of domains in the shape of long stripes as the direction of the polarization of light rotated from 0° as shown in the Fig. 3c.

Two types of domains were visible from the pictures; domain A is no stripe feature and domain B is the stripe feature. T_A and T_B are the transmitted light intensities from domain areas A and B, respectively, and plotted as a function of angle of polarization shown in Fig. 3d (top panel). The transmission intensities from domains A and B oscillate with 180° periodicity, indicating linear dichroism with the 120° phase difference between these two domains. Figure 3 d (bottom panel) shows the difference of transmitted light intensities of the two domains ($T_B - T_A$) as a function of angle of polarization. The solid line is the theoretical fit to the equation $(T_B - T_A) = \sqrt{3}\omega I \sin(2\phi)$ where ω is the transmission coefficient and I is the intensity of the incident light. The contrast between A and B domains disappears at the polarization angle of 0, 90, 180, and 270° ($T_B - T_A = 0$) due to the linear dichroism of the domains which matches with the fitted equation. Figure 3 e shows the domain schematic with optical axes. The domain structure in In₂Se₃ is reported to be very stable at ambient conditions. Even in 60 days, it shows the robust nature of stable ferroelectric applications. Imaging with low energy electron microscopy (LEEM) using micro low energy electron diffraction (μ -LEEM) experiment, it is found that the each domains are formed by a 1D superlattice structure along any one of the three equivalent close-packed directions of the hexagonal c-plane. The diffraction patterns demonstrate that In₂Se₃ samples belong to the β' phase [53]. The domain also shows tunable properties as a function of temperature. The domains disappear with heating and completely disappear at 204°C Interestingly, the domains are recovered after cooling the sample, which is a completely reversible process. This also confirms the phase change of the materials from β (204°C) to β' (domain) phase. This continuous phase transition indicates that the β to β' phase transition is of second-order phase transition. In another case, to examine ferroelectricity in the β' phase, Zheng et al. [52] used Piezoelectric force microscopy (PFM) technique at room temperature. Figure 4 a shows the atomic force microscopy (AFM) surface topography image of the exfoliated sample. Figure 4 b and c show the PFM out of plane magnitude, and phase image of the sample shows no vertical piezoelectric signal suggesting that the material does not exhibit out-of-plane ferroelectricity. In contrast, in-plane PFM images shown in Fig. 4d (magnitude) and Fig. 4e (phase) show strong signal with stripe domain features similar to the domain observed in optical measurements in Fig. 3. The results verified the existence of ferroelectricity in the materials in in-plane and not in the out-of-plane directions. From the dichroism and PEEM experimental contrast, it sketched the polarization of each domain and displayed it in Fig. 4f. This study confirms the stable ferroelectric behavior on In₂Se₃ thin layers down to 45 nm thick at room temperature with a Curie temperature up to 200°C.

Fig. 3 Linear dichroism of In_2Se_3 . **a** Crystal structure of layered $\beta\text{-In}_2\text{Se}_3$. **b** Schematic of the linear polarization optical microscopy measurement. **c** Optical image sequence of $\beta\text{-In}_2\text{Se}_3$ imaged by light of different polarization angles. Scale bar, 25 μm . **d** Polarization angle dependence of the light transmission of the regions A and B as shown in **c** a.u., arbitrary units. **e** Schematic of the optical axes of regions A and B. The figures are obtained with permission from Reference [52]

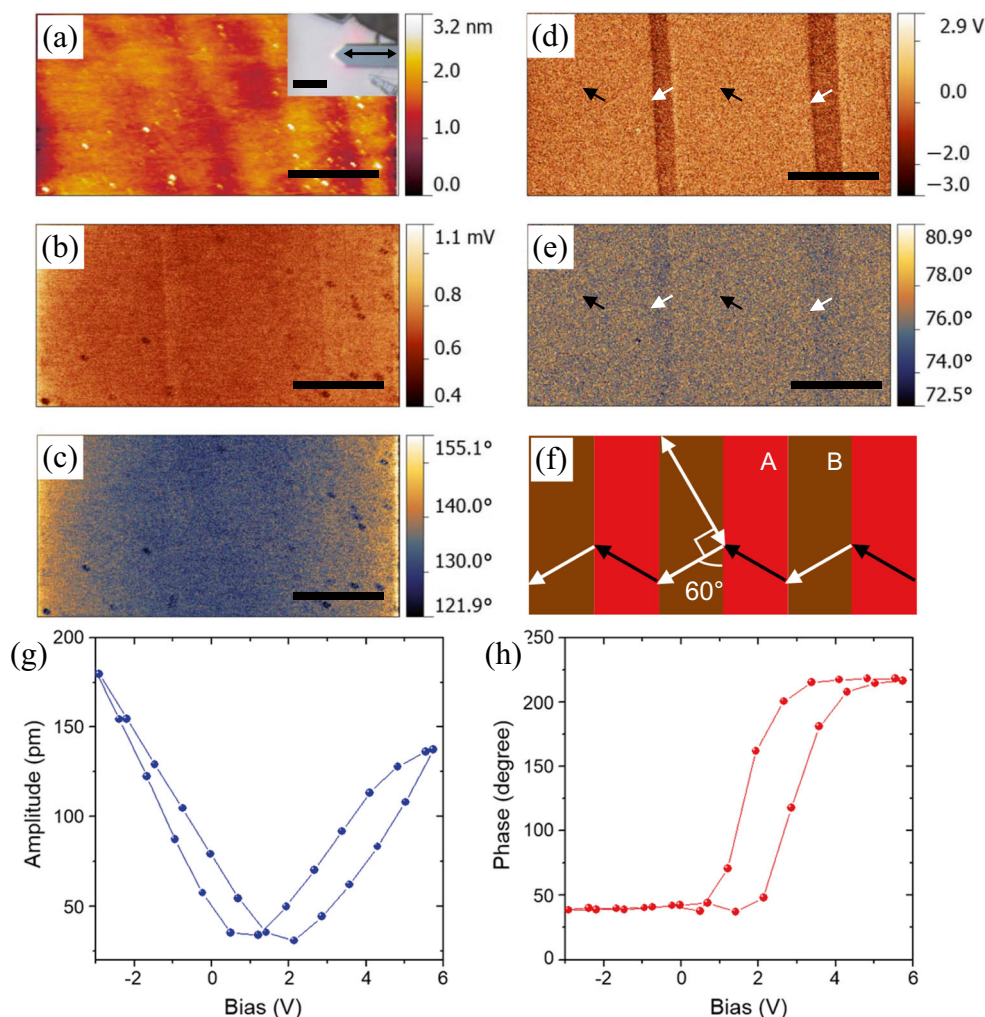


A similar ferroelectric behavior was studied in $\alpha\text{-In}_2\text{Se}_3$ thin film [55–57], which shows in-plane and out-of-plane ferroelectric behavior. Multiple conductance states were induced in $\alpha\text{-In}_2\text{Se}_3$ -based ferroelectric semiconducting field-effect transistor (FeSFETs) by controlling the out-of-plane polarization, which permits the device to faithfully mimic bio-synaptic behaviors. In addition, an abnormal resistive switching phenomenon was also reported when operated in the in-plane ferroelectric switching mode. FeSFETs offer advantages over conventional ferroelectric gate insulators because the hysteresis and multiple conductance states are implemented by control over the intrinsic ferroelectric switching of the channel material, which allows it to alleviate the constraint on complex gate stacks in FeSFETs, besides leakage current and short retention times of gate ferroelectrics.

Similarly, in another report, out of plane domains with opposite polarizations are visualized by PFM measurements in $\alpha\text{-In}_2\text{Se}_3$ flakes [54]. Single-point poling experiments suggest that the polarization is potentially

switchable for $\alpha\text{-In}_2\text{Se}_3$ nanoflakes with thicknesses down to ~ 10 nm. The PFM hysteresis loops at individual points of the $\alpha\text{-In}_2\text{Se}_3$ flakes was measured on a 20-nm thick sample presented in Fig. 4 g and h, where a stiff cantilever with a spring constant of 40 N/m was used and the DC bias voltage was swept between -3 V and $+6$ V with an AC voltage of 800 mV. The amplitude response shows a butterfly loop in Fig. 4g with an opening of ~ 1.5 V, whereas the phase switches 180° at the same turning points. The corresponding phase hysteresis loop also presented in Fig. 4h. The unsaturated amplitude signal is likely due to the significant leakage (high concentration of free carriers) of the samples, although it is difficult to exclude the possibility of surface charging and other possible extrinsic effect. The piezotronic effect is also demonstrated in two-terminal FET devices, where the Schottky barrier was modulated by the strain-induced piezo-potential. This demonstrated that the $\alpha\text{-In}_2\text{Se}_3$ has potential application for piezotronics.

Fig. 4 PFM measurements. **a** AFM topography image of β' - In_2Se_3 . Inset: optical image of the cantilever and the exfoliated crystal. The horizontal scanning direction is indicated by the black double-headed arrow. **b** and **c** PFM amplitude and phase of vertical signal. **d** and **e** PFM amplitude and phase of lateral signal. **f** Schematic of the example optical axis (white double-headed arrow) and ferroelectric polarization directions (white/black arrows) of the domains. Scale bars, 5 and 30 μm (inset). **g** and **h** display the polarization reversal under an external electrical field. On-field (**g**) PFM amplitude and (**h**) PFM phase hysteresis loops on a 20-nm thick flake. (**a**)–(**f**) obtained with permission from Reference [52] and (**g**) and (**h**) obtained from Reference [54]



5 Ferroelectricity and domain wall structure in monolayer SnSe

Microscopic imaging and controlled manipulation of the out-of-plane polarization in few atomic layer ferroelectric materials via PFM have been demonstrated above in In_2Se_3 and also reported in layered materials like MoTe_2 and CuInP_2S_4 [42, 57–59]. However, although PFM studies of in-plane ferroelectricity have been reported in several Van der Waals-layered materials, PFM studies of in-plane polarized ferroelectrics have not reported in the single atomic layer thick sample due to the difficulty in the measurement associated with AFM tip. The in-plane component of the electric field which is sensed by the AFM tip is much weaker than the signal out of plane. On the other hand, the imaging of in-plane polarization in 2D ferroelectric in a monolayer sample is relatively easy for scanning tunneling microscopy (STM) method.

Figure 5 presented a variable temperature STM scanning method to controllably switch the in-plane polarization via domain manipulation in single atomic layer SnSe sample at

room temperature and demonstrated its ferroelectric transition temperature to be as high as 380–400 K, close to that of BaTiO_3 [61]. Figure 5 a and b show that the topographic and dI/dV mapping images clearly display opposite charge accumulation on the surface of SnSe from one side to another with red and blue contrast resulting from band bending. Figure 5 a displays the topography image of height contrast 1 Å that verified the monolayer of the SnSe. Figure 5 b shows the contrast of conductance $dI/dV = 0.6$ pS with ratio of the conductance for up and down polarization $(dI/dV)_{\text{up}} / (dI/dV)_{\text{down}} = 2.3$ which both confirms the in-plane polarization. Figure 5 c shows that the 180° domain wall (straight white line) separates the two domains (black arrows) with opposite in-plane polarity. Figure 5 d shows the zig-zag domain wall with tail-to-tail connection (white lines) and forms three domains on the surface. Interestingly, they manipulated the ferroelectric domain walls by applying a pulse of electric field, which is discussed below.

Figure 6 a shows the schematic of applying voltage pulse to the sample through STM tip $d_0 = 20$ nm distance far from the

Fig. 5 Ferroelectric domain study through STM tip on monolayer SnSe sample at room temperature. **a** AFM topography image and **b** recorded dI/dV image of the monolayer SnSe flake at $V_s = -0.2$ V, $I_t = 2$ pA. **c** and **d** are the dI/dV image which shows straight and zig-zag domain walls, respectively, measured at $V_s = -0.2$ V, $I_t = 2$ pA for (c) and $V_s = -0.35$ V, $I_t = 2$ pA for (d). DWs are indicated by white dashed lines. The figures are obtained with permission from Reference [60]

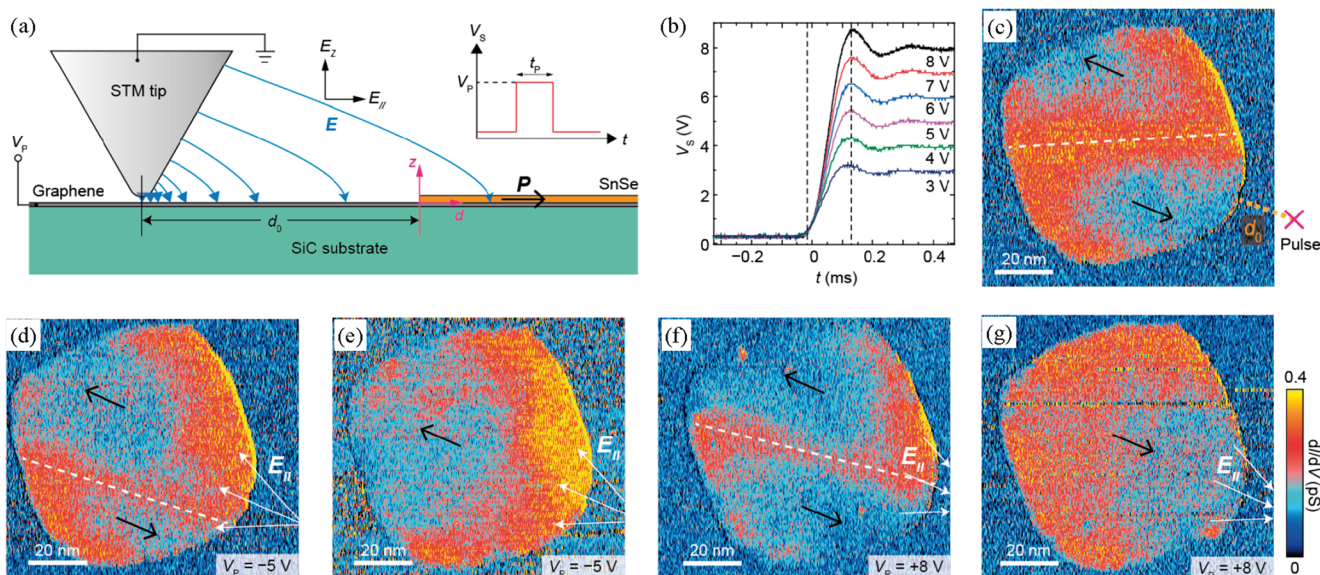
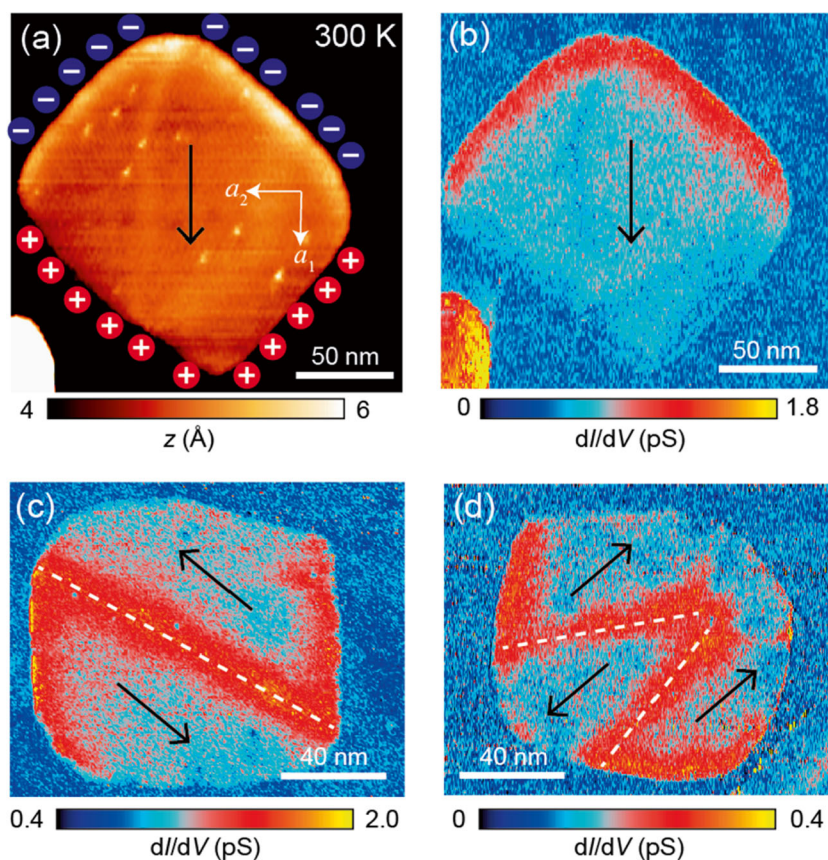


Fig. 6 Controllable ferroelectric switching of SnSe monolayer. **a** Schematic of ferroelectric switching achieved by applying a bias voltage pulse V_p at a point on the graphene substrate close to a SnSe monolayer plate. The corner of SnSe closest to the STM tip was set as $d = 0$, and the upper surface of graphene was set as $z = 0$. **b** Rising edges of the bias voltage pulses. Dashed lines indicate the onset and maximum values of the bias voltage. **c–g** Consecutive dI/dV images of a

ferroelectric switching sequence in a SnSe monolayer plate. Set points: $V_s = -0.35$ V, $I_t = 2$ pA. The pulses were applied at the same point indicated in (c). The widths of all the pulses were 50 ms. The direction of the in-plane components of tip-induced electric fields is indicated by the white arrows. All of the data in this figure were collected at room temperature. The figures are obtained with permission from Reference [60].

sample edge, where SnSe was placed on the metallic graphene sheet. The applied pulse width was 0.14 ms, which is much longer than the relaxation time of the charge carriers in graphene, which is 250–450 fs; thus, the electric field induced by the pulse can be regarded as quasi-static. The duration of the pulse voltage is 50 ms (Fig. 6b). Figure 6c shows the 180° DW which separates the two domains of opposite polarity. The cross mark indicated the position of the applied voltage pulse at distance $d_0 = 20$ nm from the edge of the sample. By applying the voltage pulse of $V_p = -5$ V, the 180° DW was pushed away from the middle of the sample to the side as shown in the Fig. 6d. The domain of polarization direction along the direction of the applied electric field expanded by pushing the DW towards the domain of opposite polarity of the applied electric field. Applying a second voltage pulse of $V_p = -5$ V, the 180° DW completely pushed to the edge of the sample and annihilated the 180° DW completely and changed to a single domain as shown in the Fig. 6e with polarization following the direction of the applied electric field. The voltage pulse not only annihilates the DWs but also rotates the DWs to different angles. Author also showed that the 180° DWs can be created by applying the voltage pulse with opposite polarity. In Fig. 6f, by applying $V_p = +8$ V, they created again a new 180° DW with two domains of opposite polarity. When they applied a second voltage pulse of $V_p = +8$ V, the newly created 180° DW pushed to the edges and annihilated to form a single domain with the polarization following the direction of the applied electric field [Fig. 6g]. The great control over the DWs creation and annihilation leads to the application of these materials as domain or DW-based non-volatile memory devices in many electronics. Each polarity of the domains and each different configuration of the DWs have potential to store data providing the opportunity to store multiple data in one structure for the application of random access memory devices.

2D ferroelectrics have a unique polarization profile which does not exist in oxide perovskite ferroelectrics. They may exhibit in quadruple-well ferroelectric Van der Waals crystals reported recently by Brehm et al. [62] in copper indium thiophosphate (CuInP_2S_6). It is shown that the potential energy for Cu displacements is strongly influenced by strain in accounting for the origin of the ferroelectricity. The low- and high-polarization states depend upon the magnitude of the displacement of Cu atoms. The low-polarization (LP) state was achieved by small displacement of Cu atom (1.62 Å) corresponding to the polarization $P = \pm 4.93 \mu\text{C}/\text{cm}^2$. Similarly the high-polarization (HP) state was obtained by the displacement of Cu ion to ~ 2.25 Å corresponding to $P = \pm 11.26 \mu\text{C}/\text{cm}^2$. Depending upon the alignment of the ferroelectric domains (polarization) either parallel or antiparallel, one can achieve four different polarization states giving multi-well ferroelectricity. These polarization states can be tuned by the temperature, pressure, and bias voltage.

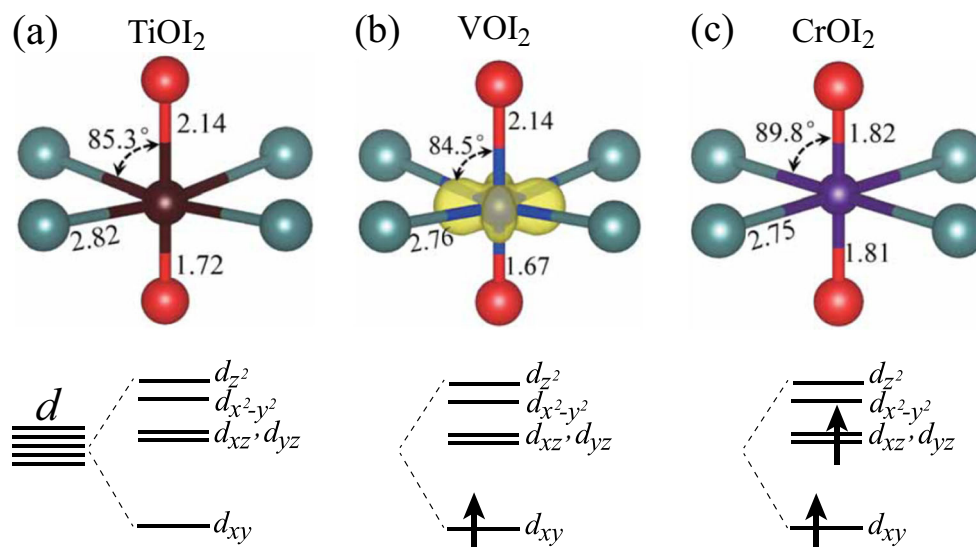
2D material with coexistence of reversible polar distortion and metallicity leads to ferroelectric metal. For piezoelectricity, noncentrosymmetric crystal structure is the only requirement. In contrast, for a polar material to show ferroelectric behavior, noncentrosymmetric and existence of a unique polar axis are required. A material to be considered ferroelectric, it needs both polar to show bistability of the polarization along the polar axis. Traditionally, ferroelectricity has been observed in materials that are insulating or semiconducting rather than metallic because conduction electrons in metals screen out the static internal fields arising from a long-range dipolar order. There was long sought for the understanding of the existence of both metallicity and ferroelectricity in a single phase of the materials. Recently, Sharma et al. [63] observed the coexistence of metallicity and ferroelectricity in the bulk single crystal WTe_2 at room temperature. WTe_2 single crystal is a material from transition metal dichalcogenide groups with orthorhombic phase and shows metallic behavior [64]. This material also shows Shubnikov-de Haas van oscillation (SdH) due to its high carrier mobility. Sharma et al. [63] demonstrated the existence of ferroelectric switchable domain walls using PFM measurements and by applying external electric fields. They also demonstrated theoretically using DFT calculation that the anisotropy of the crystal structure of WTe_2 plays an important role for showing the ferroelectricity. A 2D material that is both metallic and ferroelectric in its bulk crystalline form at room temperature has the potential application for new nanoelectronics.

6 Two-dimensional multiferroics in violation of the d^0 rule

The existence of coupling between magnetism and polarization is the key physical property of multiferroic materials. The origin and mechanism behind the multiferroic can be very different in a plethora of multiferroic materials systems and need to be investigated. The magnetic moments for any magnetic materials originate from the partially occupied unpaired d and/or f orbital electrons. For the formation charge dipole, it needs to have empty d-orbitals to satisfy the condition of coordinate bond which is called the d^0 rule. Tan et al. [65] studied the two-dimensional multiferroics in violation of the d^0 rule using first principle calculations.

This violation d^0 rule is required to see both ferroelectricity and magnetism behavior. Multiferroic properties of monolayer materials (TiOI_2 , VOI_2 and CrOI_2) with the combination of Type I multiferroics (the origin of ferroelectricity and magnetism in large polarizations and very weak magnetoelectric coupling at high transition temperatures) [66] and Type II multiferroics (ferroelectricity is a derivative of magnetism in small polarizations and strong magnetoelectric coupling at low transition temperatures) are discussed [66]. The local

Fig. 7 2D multiferroics in violation of the d^0 rule. Local geometries of (a) TiO_2 , (b) VOI_2 , and (c) CrOI_2 . The bond lengths (in Å) and O-metal-I bond angles are denoted. Lower panels: the corresponding d-orbital splitting and occupation, where an arrow means an electron. In (b), at the center, the decomposed charge density of the occupied d_{xy} orbital is plotted in yellow color with an isosurface of 0.018 e/Bohr^3 . The figures are obtained with permission from Reference [65].



geometries of the (a) TiO_2 , (b) VOI_2 , and (c) CrOI_2 are shown in Fig. 7. In TiO_2 , d orbital is absent which is consistent with the d^0 rule (Fig. 7a lower panel). The origin of ferroelectricity is the same with the perovskite BaTiO_3 [67] due to the d^0 nature of the Ti ions. This happens due to the soft phonon mode associated with covalent bonds between Ti and anions. In VOI_2 , d_{xy} singlet is occupied and distributed in the plane perpendicular to the V-O chain (Fig. 7b lower panel). The occupation of d orbital increases the ferroelectric polarization in VOI_2 because of an extra d electron in V and the d orbital cation splits into four subgroups [65]. Two features can be distinguished in VOI_2 , Type I and type II multiferroics. One is the presence of conventional polarization for Type I multiferroics. Another is that the occurrence of both ferroelectric and magnetic properties arises due to the same V cation and parasitic nature of polarization from the d orbitals for Type II multiferroics. Such type of duality in VOI_2 makes it possible to combine large polarization as well as strong magnetoelectric coupling. If one more d electron is added, the occupation of d_{xz}/d_{yz} will occur which causes the suppression of polarization. This is shown in CrOI_2 monolayer (Fig. 7c) where the off-center displacement of the Cr cation is almost removed with bond angle O-Cr-I close to 90° . Thus, CrOI_2 is a half-metal [65]. The violation d^0 rule in VOI_2 shows the interesting ferroelectricity and ferromagnetism while TiO_2 does not violate d^0 and shows only ferroelectric nature.

7 Multiferroicity double-perovskite (DP) bilayer RP structure $\text{Ca}_3\text{FeOsO}_6$

The Ruddlesden-Popper (RP) phase [69] having general formula $\text{A}_{n+1}\text{B}_n\text{X}_{3n+1}$ where A (alkali metal, alkali earth metal, rare earth metal) and B (transition metal) are cations, X is an anion i.e., oxygen, and n is the number of octahedral layers

like perovskite stack [70] which possess interesting properties such as colossal magnetoresistance, ferroelectricity, ferromagnetism, and multiferroics. The transition metals which have partially filled d orbitals in the B-site play important roles for the useful properties. Recently, the B-site substituted double-perovskite (DP) bilayer RP structure of the type $\text{A}_3\text{B}_2\text{O}_7$ has been of great interest among researchers due to its high ferroelectric polarization [69, 70]. Zhang et al. [68] studied the designing of the two-dimensional multiferroics with the coupling of polarization and magnetization by taking a double-perovskite (DP) bilayer $\text{Ca}_3\text{FeOsO}_6$ where Ca is at A-site Fe and osmium (Os) are at B-site and X is an anion as per RP phase. The transition metal ions at the B-site have the rock-salt structure [71]. This B-Site-ordered DP oxide in Fig. 8 a shows the magnetic anisotropy calculation of $\text{Ca}_3\text{FeOsO}_6$, and it shows that the easy-magnetization axis always lies in the plane perpendicular to the polarization. The direction of the easy axis changes slightly when Dzyaloshinsky-Moriya (DM) interaction is taken into account [72, 73]. This type of changes is similar to the reported prototype multiferroic BiFeO_3 where the antiferromagnetic plane is always perpendicular to the polarization [74]. Further, in $\text{Ca}_3\text{FeOsO}_6$ bilayer, the polarization reversal yields a change in a direction symmetric about the c-axis to its original direction. As polarization reverses, switching magnetization leads to the reversal of the in-plane and out-of-plane magnetization [as in Fig. 8b]. Figure 8 c shows the magnetic anisotropy energy surface of a series of intermediate structures along the switching path from the initial state to the orthogonal twin state. It is seen that the easy axis rotates continuously around the c axis. This type of change with respect to the initial state is related to the magnetic phase transition. From the above results, the magnetization direction always changes in the upper hemisphere without crossing the ab plane and magnetization can be reversed in ferroelectric switching in-plane. The coexistence of

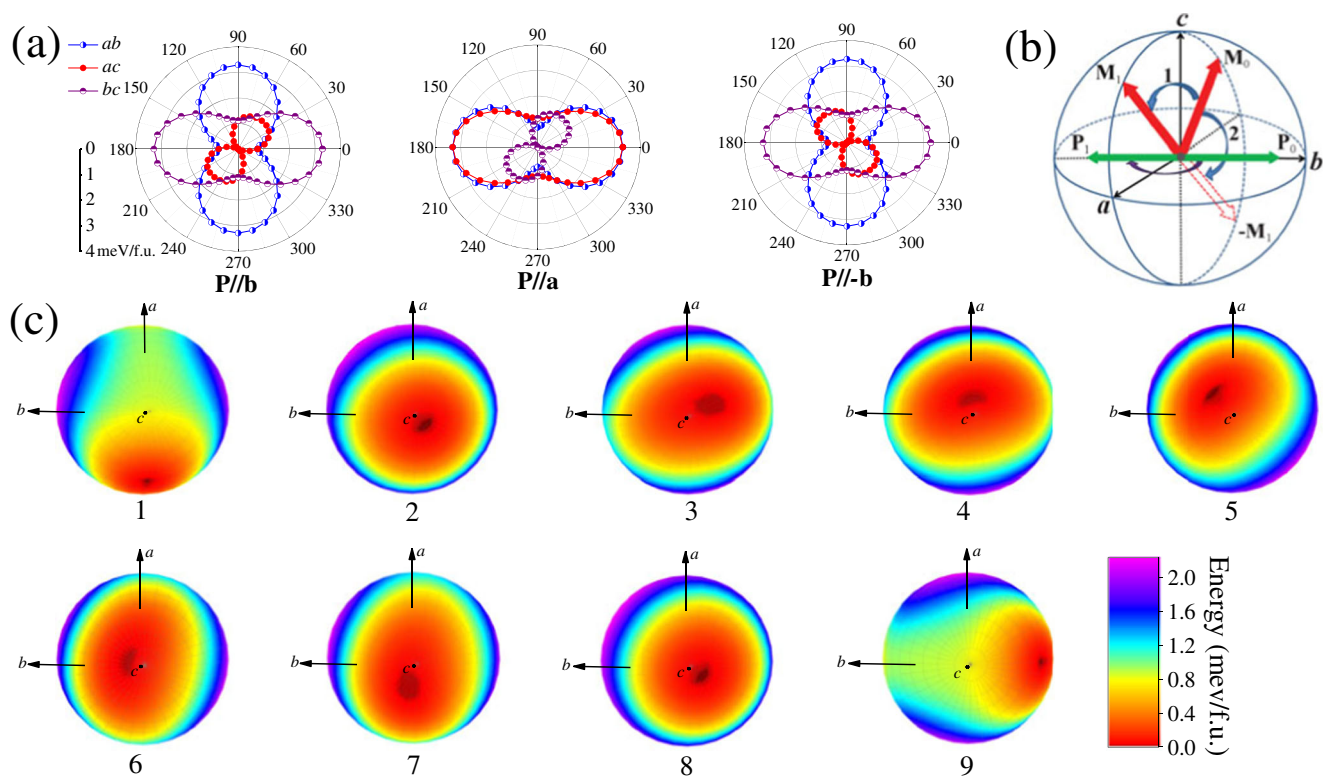


Fig. 8 Magnetic anisotropy calculation of double-perovskite (DP) bilayer RP structure $\text{Ca}_3\text{FeOsO}_6$ where Fe and Osmium Os are at the B-site: **a** magnetic anisotropy energy of the initial (P//b), orthogonal twin (P//a), and final (P//b) states in ferroelectric polarization switching, where P represents the ferroelectric polarization. Here, the change in energy is shown as a function of the angle between the spin direction and the basis

vector. When the spins lie in the ab (ac) and bc planes, the angle refers to the a and b axes respectively. **b** Schematic diagram of the change of direction of magnetization with the reversal polarization. **c** Magnetic anisotropy energy surface of a series of intermediate structures along the switching path from the initial state to the orthogonal twin state. The figures are obtained with permission from Reference [68].

ferroelectricity and ferromagnetism along with the mechanism of magnetoelectric coupling is also theoretically verified in the DP bilayer $\text{Ca}_3\text{FeOsO}_7$ [68].

8 Multiferroic properties of iron-doped 2D In_2Se_3

Yang et al. [75] have studied the iron-doping induced multiferroic in two-dimensional In_2Se_3 , i.e., $\text{Fe}_{0.16}\text{In}_{1.84}\text{Se}_3$ (FIS). Theoretical and experimental study confirms the multiferroic nature in $\text{Fe}_{0.16}\text{In}_{1.84}\text{Se}_3$ (FIS). The synthesized exfoliate flake of FIS was initially investigated via PFM study and presented in Fig. 9a–d. Figure 9 a shows the AFM topography image of the exfoliated flakes of having several numbers of layers on a Pt/Si substrate.

The corresponding polarization phase image shown in Fig. 9b reveals that two color contrasts verified the two opposite out of plane polarizations (up and down) originated from the 2D flakes. These two ferroelectric domains from the sample upward and downward polarization were also manipulated by applied electric fields and simultaneously measuring the phase image. Figure 9 d shows the two squares of two distinct

regions biased by applied opposite voltages (−5 V and +6V) by the metallic AFM tip and scanned over the sample. As one can see the two distinct phase contrasts from the region of negative and positive applied voltage indicate the two different out of plane polarizations of the sample. Thus, one can manipulate the polarization of the sample whether it’s upward or downward by selecting ±Ve bias voltage, which can be used to read and write the information for nonvolatile memory devices. The domain manipulation is also demonstrated by acquiring the PFM amplitude as a function of applied bias voltage between the AFM tip and the conducting substrate. The amplitude and phase signals were plotted in Fig. 9d as a function of applied bias from −5V to +5V. The butterfly-like amplitude and hysteresis phase signal indicate that the domains can be easily reversed from upward to downward or vice versa by just applying ±5V bias voltage perpendicular to the 2D surface of the FIS. Further, the magnetic properties of FIS are explored at low temperature. The magnetic measurements of undoped In_2Se_3 show diamagnetic behavior [Fig. 9e], whereas doped crystal $\text{Fe}_{0.16}\text{In}_{1.84}\text{Se}_3$ (FIS) shows ferromagnetic behavior with anisotropy along parallel and perpendicular to the 2D plane measured at 2 K [Fig. 9g]. The Curie temperature of the FIS measured using FC and ZFC shows T_C

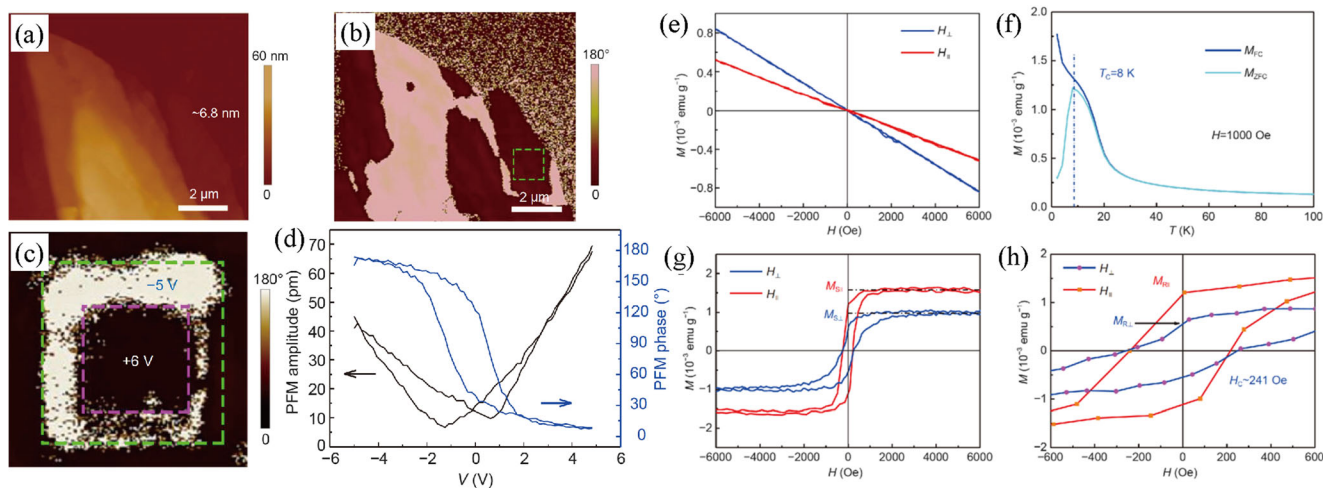


Fig. 9 Ferroelectric and ferromagnetic characterizations of Fe-doped 2D In_2Se_3 crystals. **a** AFM topography image of the flake containing various layers. **b** The PFM phase image. **c** Phase image of 6.8 nm thick flake shows out of plane polarizations at applied voltage -5 V and $+6\text{ V}$. **d** PFM amplitude data of a 20-nm thick flake as a function of sweeping voltage from -6 V to $+6\text{ V}$ shows hysteresis loops. **e** Magnetic hysteresis loops at

2 K for undoped In_2Se_3 . **f** Field-cooled and zero-field-cooled magnetization as a function of temperature for $\text{Fe}_{0.16}\text{In}_{1.84}\text{Se}_3$ (FIS) from 2 to 100 K. **g** Magnetic hysteresis loops of FIS, when the applied magnetic field is in parallel and perpendicular to the 2D plane measured at $T = 2\text{ K}$. **h** Expanded view of the loop of $\text{Fe}_{0.16}\text{In}_{1.84}\text{Se}_3$ (FIS) in (g). The figures are obtained with permission from Reference [75]

$\sim 8\text{ K}$ [shown in Fig. 9f]. The expanded view of the M-H loop is shown in Fig. 9h. The saturation magnetization $M_S = 9.77 \times 10^{-4}\text{ emu g}^{-1}$ (in the perpendicular) and $M_S = 1.57 \times 10^{-3}\text{ emu g}^{-1}$ (in parallel direction) of the magnetic field. The remnant magnetization $M_R = 5.52 \times 10^{-4}\text{ emu g}^{-1}$ (in perpendicular direction) and $M_R = 1.16 \times 10^{-3}\text{ emu g}^{-1}$ (in parallel direction) of magnetic field for FIS. The coercivity field measured from the M-H loop is $H_c = 241\text{ Oe}$ and is the same for both perpendicular and parallel direction. The origin of the magnetization, which is also investigated using first-principles based theoretical DFT calculation, confirms the ferromagnetism. The predicted magnetic moment of the FIS sample is $5\text{ }\mu_B$ per Fe atom when Fe substitutes In atoms in In_2Se_3 [75]. The Fe substitution in pristine In_2Se_3 alters the magnetic as well as ferroelectric properties of the material to show multiferroic nature.

There have been a number of 2D multiferroics predicted with the co-existence of ferroelectricity and ferroelasticity and ferromagnetism and ferroelasticity [76–80]. Recently, some artificial multiferroics have been developed. Lu et al. [81] studied the artificial 2D multiferroics through Van der Waals (vdW) heterostructure formed by FM bilayer chromium tri-iodide (CrI_3) and FE monolayer Sc_2CO_2 with enhanced magnetoelectric effect and can be useful for nanoelectronics. Gong et al. [82] predicted that two-dimensional multiferroics show switching ON and OFF behavior through heterostructure by stacking the atomic layers of ferromagnetic $\text{Cr}_2\text{Ge}_2\text{Te}_6$ and ferroelectric In_2Se_3 for logic applications. This indicates the strong magneto-electric coupling between ferromagnetic and ferroelectric layers.

Magnetic tunneling junctions (MTJs) are the key building blocks of non-volatile random access memory devices (MRAMs). The basic principle of this MTJ is changing the relative magnetoresistance, called tunnel magnetoresistance (TMR) between two ferromagnetic layers with the orientation of their spin moments. MTJ consists of two magnetic layers separated by a thin insulating layer, where the changes of magnetic alignments in the two ferromagnetic layers from parallel to antiparallel causes the sizable change in TMR, which has tremendous application in data storage and memory devices. This MTJ effect can be enhanced using a ferroelectric barrier layer between two ferromagnetic layers. The benefits of introducing a ferroelectric barrier layer between two ferromagnetic layers are the coupling effect between electric polarization and magnetic moments at the interface. The electric polarization can be tuned by applying an electric field, which produces a sizable change in resistance of the junction, called tunneling electrostatic resistance (TER) and this phenomenon could enhance the TMR effect in MTJ. Recently, Su et al. [83] have theoretically demonstrated a tunnel junction by introducing a thin 2D ferroelectric layer of In_2Se_3 between two layers of 2D magnetic materials Fe_mGeTe_2 and Fe_nGeTe_2 , where $m, n = 3, 4, 5$ and $m \neq n$ are called multiferroic tunnel junctions (MFTJs). Out of plane or in-plane ferroelectric polarizations of In_2Se_3 has been achieved by applying in-plane or out of plane electric fields [57]. Thus, we can realize a novel MFTJ by introducing In_2Se_3 between two Fe_nGeTe_2 layers. Parallel and antiparallel magnetization alignment between two ferromagnetic layers and weak exchange interaction between them was controlled through a thin ferroelectric In_2Se_3 layer. Therefore, nonvolatile multiple states with switchable

ferroelectric polarization of In_2Se_3 can be realized. Further, theoretically it also investigated the TMR effect in Van der Waals MTJs which consist of ferromagnetic electrodes (Fe_3GeTe_2) and a graphene or hexagonal boron nitride (h-BN) layer. These MTJs depend on the spin electronic structure of ferromagnetic Fe_3GeTe_2 electrodes. Further investigations are required to understand the intrinsic properties of 2D vdW MTJs for spintronics applications [84]. In addition to this, the Table 1 contains a number of recently developed 2D ferroelectric and multiferroics using theoretically as well as experimental techniques.

9 Challenges, opportunity, and future direction

Ferroelectric materials with stable and switchable spontaneous polarization and can be controlled by an external electric field are potential candidates for many technological applications,

including nonvolatile memories, field-effect transistors, solar cells, and sensors. The nanoscale ferroelectrics have been well proven by many theoretical predictions. However, it should be mentioned that either the careful selection of the substrate to grow the materials with less lattice mismatch is required for fabricating high-quality ferroelectric thin films at the nanoscale level. This might need a lot of time to overcome this challenge. Though 2D ferroelectric materials were predicted long before, there are still huge challenges to be observed in stable polarization along the plane and out of the plane in atomic layer materials. The ability to preserve pristine nature of 2D ferroelectricity and producing defect-free materials are the great challenge to the scientific community and need to be addressed for practical applications. The integration of 2D materials with three-dimensional (3D) systems is still a significant challenge, limiting device performance and circuit design [94].

The successive study on structure, electronic, ferroelectrics, and magnetism of 2D oxyhalide VOF_2 and VOI_2 monolayer

Table 1 The recent development of 2D ferroelectric and multiferroics using theoretically as well as experimental techniques

Materials	Type	Curie temperature (T_C)	Mechanism	Year and reference
CuInP_2S_6	Ferroelectric	320 K	Structure distortion	2016 [59]
CuInP_2S_6	Ferroelectric	Room temperature and above	Ion displacement	2020 [62]
SnTe	Ferroelectric	270 K	Structure distortion	2016 [85]
GeSe	Ferroelectric	2300 K	Structure distortion	2016 [86]
SnSe	Ferroelectric	Room temperature and above	Structure distortion	2016 [86]
SnSe	Ferroelectric	380–400 K	Domain walls by external applied pulse voltage	2020 [60]
GeS	Ferroelectric	6400 K	Structure distortion	2016 [86]
SnS	Ferroelectric	1200 K	Ion displacement	2016 [86]
$\alpha\text{-In}_2\text{Se}_3$	Ferroelectric	Room temperature	Structure distortion	2017 [54]
$\alpha\text{-In}_2\text{Se}_3$	Ferroelectric	Room temperature	Dipole effect	2018 [56]
In_2Se_3	Ferroelectric	700K	Dipole locking/covalent bond configuration	2018 [57]
$\alpha\text{-In}_2\text{Se}_3$	Ferroelectric	Room temperature	Structure distortion	2018 [87]
$\alpha\text{-In}_2\text{Se}_3$	Ferroelectric	Room temperature	Dipole Effect	2018 [88]
$\beta'\text{-In}_2\text{Se}_3$	Ferroelectric	473 K	Structure distortion	2018 [52]
2H $\alpha\text{-In}_2\text{Se}_3$	Ferroelectric	Room temperature	Non-equivalent interlayer spacing	2018 [89]
WTe_2	Ferroelectric	350 K	Electron-hole correlation effects	2018 [42]
BA_2PbCl_4	Ferroelectric	453 K	Structure distortion	2018 [90]
d1T- MoTe_2	Ferroelectric	Room temperature	Structure distortion	2019 [47]
$\text{Bi}_2\text{O}_2\text{Se}$	Ferroelectric	Room temperature	Structure distortion	2019 [91]
$\beta'\text{-In}_2\text{Se}_3$	Antiferroelectric	Room temperature	Lattice distortion	2020 [92]
BLG/BN	Ferroelectric	4K	Moiré Heterostructure	2020 [43]
GeS	Multiferroic	Room temperature	Structure distortion	2016 [93]
SnS	Multiferroic	Room temperature	Structure distortion	2016 [93]
GeSe	Multiferroic	Room temperature	Structure distortion	2016 [93]
SnSe	Multiferroic	Room temperature	Structure distortion	2016 [93]

with the coexistence of both ferroelectricity and ferromagnetism has been demonstrated theoretically but required experimental work to confirm this theoretical finding. The existence of ferroelectricity in VOI_2 is due to the violation of d^0 rule. There might be several other materials that need to be investigated which were in the same category of violation of d^0 rule. It needs experimental investigation of ferroelectricity and ferromagnetism as well as magnetoelectric effect for conventional multiferroics. Further, we discussed a theoretical prediction of multiferroic properties with strong magnetoelectric coupling of double-perovskite bilayer $\text{Ca}_2\text{FeO}_5\text{O}_6$ RP structure. A systematic experimental study is sought for thorough understanding of anisotropic nature and its role in the multiferroic properties.

The room temperature out-of-plane ferroelectricity is observed in the monolayer MoTe_2 using theoretical calculation as well as experimental findings. This also shows Curie temperature above room temperature. Still, there is a huge challenge to understand the stability of ferroelectricity in monolayer samples. The interaction of monolayer with the substrate plays an important role to maintain the ferroelectric nature and needs further investigation. The substitution of Fe in the site of In_2Se_3 , i.e., $\text{Fe}_{0.16}\text{In}_{1.84}\text{Se}_3$ (FIS), exhibits ferroelectricity, and ferromagnetism simultaneously means it is a multiferroic material. But, the ferromagnetic effect is observed only at low temperature and not at room temperature, which limits the multifunctional application of this material. Therefore, developing FIS with suitable substitution of Fe in In_2Se_3 is needed which can increase the T_C of FIS. This also opens up other materials like rare-earth elements that may be doped in In_2Se_3 which can show multiferroics with T_C . There might be several 2D materials that could show multiferroic behavior with suitable doping which needs substantial future research work.

As discussed above, the discovery of stable ferroelectricity in layered In_2Se_3 materials at room temperature has potential advantage for many electronic applications. But still there are many challenges to overcome for a wide range of applications. With the applied temperature, the domain in In_2Se_3 grows very anisotropically where length of the domain grows much faster than the width giving stripe domain feature, which limits the application for high density devices. Thus, a method needs to be developed to control the size of the domains with possible nanofabrication techniques. The ferroelectricity is also not measured in very thin samples like monolayer to few atomic layers, which may have a wide range of applications in nanoelectronics such as memory, sensor, and photovoltaic as compared to the bulk. The challenging part is to grow the large area monolayer In_2Se_3 crystal. One of the critical issues for ultrathin ferroelectric materials is the depolarization effect. It is known that the ferroelectricity of conventional ferroelectric thin films is usually suppressed, as the films are thinner than a critical thickness due to the effects of a depolarizing field induced by uncompensated charges in the presence of metal

electrodes. This issue needs to be addressed with careful measurements as a function of the number of layers. It is known that all ferroelectric materials show both piezoelectric and pyroelectric effects. The phenomenon of piezoelectricity arises from the release of electric charge under the application of mechanical stress and vice-versa, and pyroelectricity comes from the release of charge due to a material's change of temperature. As we know, the 2D materials, due to their large surface to volume ratio, were prone to deform and change their electronic properties with mechanical stress as well as change in temperature. Thus, a systematic study of piezoelectric and pyroelectric properties will lead to the potential for applications in nanoscale electromechanical devices and piezotronic sensors.

Most of the 2D materials possess large density of defects, particularly chemical vapor deposition (CVD) grown samples have higher density of defects than the chemical vapor transport (CVT) grown crystals. Domain walls pinning in thin ferroelectric materials such as SnSe is an important drawback which might arise due to the defects, wrinkle, and step, non-uniformity of the sample. It was a great achievement to manipulate the DWs in a monolayer SnSe sample by applying an electric field close to the sample. The creation of DWs and annihilation could depend upon the narrow voltage range V_p applied to the sample which might also depend upon the crystal quality, fabrication defects, etc. DWs can easily be pinned at the defect side and need larger applied electric fields to switch the DWs with different chirality. Thus, reproducibility of DWs manipulation is one of the major challenges in thin layer samples. The temperature is also an important factor to destroy the DWs in high-density electronic devices. Thus, a thorough temperature-dependent study will explore the DWs evolution in thin ferroelectric materials. The quality and nature of the substrate could drastically affect the ferroelectric DWs on a monolayer sample. Flat surface with large ferroelectric coupling would be better for the DWs manipulation for a monolayer sample. The collective measurements from a large-scale sample would pave the way towards practical applications. The discovery of ferroelectric behavior in moiré heterostructure of $\text{h-BN/graphene/h-BN}$ is one of the interesting developments in the field of 2D ferroelectricity, where bilayer graphene shows hysteresis behavior as a function of applied electric field when the top and bottom h-BN are stacked in particular orientation [43]. This could lead to the exploration of the ferroelectric behavior of many other 2D heterostructure materials beyond graphene, and we might see many interesting developments in this field in the next few years. There is a great opportunity to explore new 2D ferroelectricity and multiferroics for multifunctional applications both theoretically and experimentally. One can also study two-dimensional multiferroics in violation of the d^0 rule experimentally. Also, researchers can design and develop a high-quality interface with MoS_2 2D electronic devices

particularly for field-effect transistor (FET) through experiment. One can develop and design 2D multiferroics with intrinsic magnetoelectric coupling and 2D magnetism by the application of electric field experimentally.

Funding N.R.P. acknowledged the funding support from HBCU-UP Excellent in research from NSF, NSF-DMR#1900692. One of the authors BB acknowledges the financial support from SERB under DST Fast Track Scheme for Young Scientist (Project No. SR/FTP/PS-036/2011) New Delhi, India.

Declarations

Conflict of interest The authors declare no competing interests.

References

- W. Känzig, in *Solid State Physics*, ed. by T. P. Das, D. Turnbull, E. L. Hahn. Ferroelectrics and antiferroelectrics. In Frederick Seitz (Academic Press, 1957), p. 5
- M. Lines, A. Glass principles and applications of ferroelectrics and related materials. (Clarendon Press, Oxford, 1979).
- H. Schmid, Multi-ferroic magnetoelectrics. *Ferroelectrics* **162**, 317–338 (1994)
- N.A. Hill, Why are there so few magnetic ferroelectrics? *J. Phys. Chem. B* **104**, 6694–6709 (2000)
- W. Eerenstein, N.D. Mathur, J.F. Scott, Multiferroic and magnetoelectric materials. *Nature* **442**, 759–765 (2006)
- R. Ramesh, N.A. Spaldin, Multiferroics: progress and prospects in thin films. *Nat. Mater.* **6**, 21–29 (2007)
- D.I. Khomskii, Multiferroics: Different ways to combine magnetism and ferroelectricity. *J. Magn. Magn. Mater.* **306**, 1–8 (2006)
- K.F. Mak, C. Lee, J. Hone, J. Shan, T.F. Heinz, Atomically thin MoS_2 : A new direct-gap semiconductor. *Phys. Rev. Lett.* **105**, 136805 (2010)
- S.B. Desai, G. Seol, J.S. Kang, H. Fang, C. Battaglia, R. Kapadia, J.W. Ager, J. Guo, A. Javey, Strain-induced indirect to direct band gap transition in multilayer WSe_2 . *Nano Lett.* **14**, 4592–4597 (2014)
- L. Britnell, R. Ribeiro, A. Eckmann, R. Jalil, B. Belle, A. Mishchenko, Y.-J. Kim, R. Gorbachev, T. Georgiou, S. Morozov, A.N. Grigorenko, A.K. Geim, C. Casiraghi, A.H.C. Neto, K.S. Novoselov, Strong light-matter interactions in heterostructures of atomically thin films. *Science* **340**, 1311–1314 (2013)
- N.R. Pradhan, C. Garcia, J. Holleman, D. Rhodes, C. Parker, S. Talapatra, M. Terrones, L. Balicas, S. A. McGill, Photoconductivity of few-layered p- WSe_2 phototransistors via multi-terminal measurements. *2D Mater.* **3**, 041004 (2016).
- X. Cui, G.H. Lee, Y.D. Kim, G. Arefe, P.Y. Huang, C.H. Lee, D.A. Chenet, X. Zhang, L. Wang, F. Ye, F. Pizzocchero, Multi-terminal transport measurements of MoS_2 using a van der Waals heterostructure device platform. *Nat. Nanotechnol.* **10**, 534–540 (2015)
- X. Ling, H. Wang, S. Huang, F. Xia, M.S. Dresselhaus, Proc. Natl. Acad. Sci. U. S. A., The renaissance of black phosphorus. **112**, 4523–4530 (2015)
- N.R. Pradhan, J. Ludwig, Z. Lu, D. Rhodes, M.M. Bishop, K. Thirunavukkuarasu, S.A. McGill, D. Smirnov, L. Balicas, High photoresponsivity and short Photoresponse times in few-layered WSe_2 transistors. *ACS Appl. Mater. Interfaces* **7**, 12080–12088 (2015)
- N.R. Pradhan, D. Rhodes, S. Feng, Y. Xin, S. Memaran, B.H. Moon, H. Terrones, M. Terrones, L. Balicas, Field-effect transistors based on few-layered α - MoTe_2 . *ACS Nano* **8**, 5911–5920 (2014)
- C. Garcia, N.R. Pradhan, D. Rhodes, L. Balicas, S. McGill, Photogating and high gain in ReS_2 field-effect transistors. *J. Appl. Phys.* **124**, 204306 (2018)
- N.R. Pradhan, C. Garcia, M. Lucking, S. Pakhira, J. Martinez, D. Rosenmann, R. Divan, A.V. Sumant, H. Terrones, J.L. Mendoza-Cortes, S.A. McGill, N.D. Zhigadlo, L. Balicas, Raman and electrical transport properties of few-layered arsenic-doped black phosphorus. *Nanoscale* **11**, 18449–18463 (2019)
- Y. Zhang, J. Pang, M. Zhang, X. Gu, L. Huang, Two-Dimensional Co_2S_2 monolayer with robust ferromagnetism. *Sci. Rep.* **7**, 15993 (2017)
- R.C.G. Naber, C. Tanase, P.W.M. Blom, G.H. Gelinck, A.W. Marsman, F.J. Touwslager, S. Setayesh, D.M. de Leeuw, High-performance solution-processed polymer ferroelectric field-effect transistors. *Nat. Mater.* **4**, 243–248 (2005)
- A.Q. Jiang, C. Wang, K.J. Jin, X.B. Liu, J.F. Scott, C.S. Hwang, T.A. Tang, H.B. Lu, G.Z. Yang, A resistive memory in semiconducting BiFeO_3 thin-film capacitors. *Adv. Mater.* **23**, 1277–1281 (2011)
- R.C.G. Naber, K. Asadi, P.W.M. Blom, D.M. de Leeuw, B. De Boer, Organic nonvolatile memory devices based on ferroelectricity. *Adv. Mater.* **22**, 933–945 (2010)
- G. Catalan, J.F. Scott, Physics and applications of bismuth ferrite. *J. F. Adv. Mater.* **21**, 2463–2485 (2009)
- J.F. Scott, Applications of modern ferroelectrics. *Science* **315**, 954–959 (2007)
- D.D. Fong, G.B. Stephenson, S.K. Streiffer, J.A. Eastman, O. Auciello, P.H. Fuoss, C. Thompson, Ferroelectricity in ultrathin perovskite films. *Science* **304**, 1650–1653 (2004)
- J. Junquera, p. Ghosez, Critical thickness for ferroelectricity in perovskite ultrathin films. *Nature* **422**, 506–509 (2003)
- M. Osada, T. Sasaki, Two-dimensional dielectric nanosheets: Novel nanoelectronics from nanocrystal building blocks. *Adv. Mater.* **24**, 210–228 (2012)
- R. Ma, T. Sasaki, Nanosheets of oxides and hydroxides: Ultimate 2D charge-bearing functional crystallites. *Adv. Mater.* **22**, 5082–5104 (2010)
- T. Sasaki, M. Watanabe, Osmotic swelling to exfoliation. Exceptionally high degrees of hydration of a layered titanate. *J. Am. Chem. Soc.* **120**, 4682–4689 (1998)
- J.N. Coleman, M. Lotya, A. O'Neill, S.D. Bergin P.J. King, U. Khan, K. Young, A. Gaucher, S. De, R.J. Smith, I.V. Shvets, S.K. Arora, G. Stanton, H.Y. Kim, K. Lee, G.T. Kim, G.S. Duesberg, T. Hallam, J.J. Boland, J.J. Wang, J. F. Donegan, J.C. Grunlan, G.Moriarty, A. Shmeliov, R.J. Nicholls, J.M. Perkins, E.M. Grieveson, K. Theuvsissen, D.W. McComb, P.D. Nellist, V. Nicolosi, Two-dimensional nanosheets produced by liquid exfoliation of layered materials. *Science* **331**, 568–571 (2011).
- Y. Shi, M. Osada, Y. Ebina, T. Sasaki, Single droplet assembly for two-dimensional nanosheet tiling. *ACS Nano* **14**, 15216–15226 (2020)
- Y. Ma, B. Li, S. Yang, Ultrathin two-dimensional metallic nanomaterials. *Mater. Chem. Front.* **2**, 456–467 (2018)
- X. Huang, Z. Zeng, H. Zhang, Metal dichalcogenide nanosheets: preparation, properties and applications. *Chem. Soc. Rev.* **42**, 1934–1946 (2013)
- B. Zhang, V. Cicmancovab, J.R. Pereirab, J. Kupcick, P. Kutalekd, T. Wagnera, 2D metallic tungsten material. *Appl. Surf. Sci.* **530**, 147231 (2020)
- J.W. Colson, W.R. Dichtel, Rationally synthesized two-dimensional polymers. *Nat. Chem.* **5**, 453–465 (2013)

35. J. Shamsi, Z. Dang, P. Bianchini, C. Canale, F. Di Stasio, R. Brescia, M. Prato, L. Manna, Colloidal synthesis of quantum confined single crystal CsPbBr₃ nanosheets with lateral size control up to the micrometer range. *J. Am. Chem. Soc.* **138**, 7240–7243 (2016)
36. M. Osada, T. Sasaki, Nanoarchitectonics in dielectric/ferroelectric layered perovskites: from bulk 3D systems to 2D nanosheets. *Dalton Trans.* **47**, 2841–2851 (2018)
37. M. Osada, T. Sasaki, The rise of 2D dielectrics/ferroelectrics. *APL Mater.* **7**, 120902 (2019)
38. Z. Guan, H. Hu, X. Shen, P. Xiang, N. Zhong, J. Chu, C. Duan, Recent progress in two-dimensional ferroelectric materials. *Adv. Electron. Mater.* **6**, 1900818 (2020)
39. X. Tang, L. Kou, Two-Dimensional ferroics and multiferroics: Platforms for new physics and applications. *J. Phys. Chem. Lett.* **10**, 6634–6649 (2019)
40. Z. Liu, L. Deng, B. Peng, Ferromagnetic and ferroelectric two-dimensional materials for memory application. *Nano Research* **14**, 1802–1813 (2021)
41. B. Ozdemir, V. Barone, Thickness dependence of solar cell efficiency in transition metal dichalcogenides MX₂ (M: Mo, W; X: S, Se, Te). *Sol. Energy Mater. Sol. Cells* **212**, 110557 (2020)
42. Z. Fei, W. Zhao, T.A. Palomaki, B. Sun, M.K. Miller, Z. Zhao, J. Yan, X. Xu, D.H. Cobden, Ferroelectric switching of a two-dimensional metal. *Nature*. **560**, 336–339 (2018)
43. Z. Zheng, Q. Ma, Z. Bi, S. de la Barrera, M.H. Liu, N. Mao, Y. Zhang, N. Kiper, K. Watanabe, T. Taniguchi, J. Kong, W.A. Tisdale, R. Ashoori, N. Gedik, L. Fu, S.Y. Xu, P.J. Herrero, Unconventional ferroelectricity in moiré heterostructures. *Nature* **588**, 71–76 (2020)
44. H.P. You, N. Ding, J. Chen, S. Dong, Prediction of two-dimensional ferromagnetic ferroelectric VOF₂ monolayer. *Phys. Chem. Chem. Phys.* **22**, 24109–24115 (2020)
45. I.E. Dzyaloshinsky, A thermodynamic theory of “weak” ferromagnetism of antiferromagnetics. *J. Phys. Chem. Solids* **4**, 241–255 (1958)
46. T. Moriya, Anisotropic superexchange interaction and weak ferromagnetism. *Phys. Rev.* **120**, 91–98 (1960)
47. S. Yuan, X. Luo, H.L. Chan, C. Xiao, J. Hao, Room-temperature ferroelectricity in MoTe₂ down to the atomic monolayer limit. *Nat. Commun.* **10**, 1775 (2019)
48. S. Cho, S. Kim, J.H. Kim, J. Zhao, J. Seok, D.H. Keum, J. Baik, D.H. Choe, K.J. Chang, K. Suenaga, S.W. Kim, Y.H. Lee, H. Yang, Phase patterning for ohmic homojunction contact in MoTe₂. *Science* **349**, 625–628 (2015)
49. C.H. Naylor, W.M. Parkin, J. Ping, Z. Gao, Y.R. Zhou, Y. Kim, F. Streller, R.W. Carpick, A.M. Rappe, M. Drndić, J.M. Kikkawa, A.T.C. Johnson, Monolayer Single-Crystal 1T'-MoTe₂ Grown by Chemical Vapor Deposition Exhibits Weak Antilocalization Effect. *Nano Lett.* **16**, 4297–4304 (2016)
50. M.W. Lin, I.I. Kravchenko, J. Fowlkes, X. Li, A.A. Puzosky, C.M. Rouleau, D.B. Geohegan, K. Xiao, Thickness-dependent charge transport in few-layer MoS₂ field-effect transistors. *Nanotechnology* **27**, 165203 (2016)
51. N.R. Pradhan, D. Rhodes, S. Memaran, J.M. Poumirol, D. Smirnov, S. Talapatra, S. Feng, N. Perea Lopez, A.L. Elias, M. Terrones, P.M. Ajayan, L. Balicas, Hall and field-effect mobilities in few layered p-WSe₂ field-effect transistors. *Sci. Rep.* **5**, 8979 (2015)
52. C. Zheng, L. Yu, L. Zhu, J.L. Collins, D. Kim, Y. Lou, C. Xu, M. Li, Z. Wei, Y. Zhang, M.T. Edmonds, S. Li, J. Seidel, Y. Zhu, J.Z. Liu, W.Q. Tang, M.S. Fuhrer, Room temperature in-plane ferroelectricity in van der Waals In₂Se₃. *Sci. Adv.* **4**, eaar7720 (2018)
53. J. van Landuyt, G. van Tendeloo, S. Amelinckx, Phase transitions in In₂Se₃ as studied by electron microscopy and electron diffraction. *Phys. Status. Solidi. A.* **30**, 299–314 (1975)
54. Y. Zhou, D. Wu, Y. Zhu, Y. Cho, Q. He, X. Yang, K. Herrera, Z. Chu, Y. Han, M.C. Downer, H. Peng, K. Lai, Out-of-Plane Piezoelectricity and Ferroelectricity in Layered α -In₂Se₃ Nanoflakes. *Nano Lett.* **17**, 5508–5513 (2017)
55. L. Wang, X. Wang, Y. Zhang, R. Li, T. Ma, K. Leng, Z. Chen, I. Abdelwahab, K.P. Loh, Exploring ferroelectric switching in α -In₂Se₃ for neuromorphic computing. *Adv. Funct. Mater.* **30**, 2004609 (2020)
56. C. Cui, W.J. Hu, X. Yan, C. Addiego, W. Gao, Y. Wang, Z. Wang, L. Li, Y. Cheng, P. Li, X. Zhang, H.N. Alshareef, T. Wu, W. Zhu, X. Pan, L.J. Li, Intercorrelated in-plane and out-of-plane ferroelectricity in ultrathin two-dimensional layered semiconductor In₂Se₃. *Nano Lett.* **18**, 1253–1258 (2018)
57. J. Xiao, H. Zhu, Y. Wang, W. Feng, Y. Hu, A. Dasgupta, Y. Han, Y. Wang, D.A. Muller, L.W. Martin, P. Hu, X. Zhang, Intrinsic two-dimensional ferroelectricity with dipole locking. *Phys. Rev. Lett.* **120**, 227601 (2018)
58. C. Cui, F. Xue, W.J. Hu, L.J. Li, Two-dimensional materials with piezoelectric and ferroelectric functionalities. *npj 2D Mater Appl* **2**, 18 (2018)
59. F. Liu, L. You, K.L. Seyler, X. Li, P. Yu, J. Lin, X. Wang, J. Zhou, H. Wang, H. He, S.T. Pantelides, W. Zhou, P. Sharma, X. Xu, P.M. Ajayan, J. Wang, Z. Liu, Room-temperature ferroelectricity in CuInP₂S₆ ultrathin flakes. *Nat. Commun.* **7**, 12357 (2016)
60. K. Chang, F. Küster, B.J. Miller, J.R. Ji, J.L. Zhang, P. Sessi, S.B. Lopez, S.S.P. Parkin, Microscopic manipulation of ferroelectric domains in SnSe monolayers at room temperature. *Nano Lett.* **20**, 6590–6597 (2020)
61. K. Sakayori, Y. Matsui, H. Abe, E. Nakamura, M. Kenmoku, T. Hara, D. Ishikawa, A. Kokubu, K. Hirota, T.I.T. Ikeda, Curie temperature of BaTiO₃. *Jpn. J. Appl. Phys.* **34**, 5443–5445 (1995)
62. J.A. Brehm, S.M. Neumayer, L. Tao, A. O'Hara, M. Chyasnovich, M.A. Susner, M.A. McGuire, S.V. Kalinin, S. Jesse, P. Ganesh, S.T. Pantelide, P. Maksymovych, N. Balke, Tunable quadruple-well ferroelectric van der Waals crystals. *Nat. Mater.* **19**, 43–48 (2020)
63. P. Sharma, F.X. Xiang, D.F. Shao, D. Zhang, E.Y. Tsymbal, A.R. Hamilton, J. Seidel, A room-temperature ferroelectric semimetal. *Sci. Adv.* **5**, eaax5080 (2019)
64. D. Rhodes, S. Das, Q.R. Zhang, B. Zeng, N.R. Pradhan, N. Kikugawa, E. Manousakis, L. Balicas, Role of spin-orbit coupling and evolution of the electronic structure of WTe₂ under an external magnetic field. *Phys. Rev. B* **92**, 125152 (2015)
65. H. Tan, M. Li, H. Liu, Z. Liu, Y. Li, W. Duan, Two-dimensional ferromagnetic-ferroelectric multiferroics in violation of the d⁰ rule. *Physical review B* **99**, 195434 (2019).
66. D. Khomskii, Classifying multiferroics: Mechanisms and effects. *Physics* **2**, 20 (2009)
67. H.D. Megaw, Origin of ferroelectricity in barium titanate and other perovskite-type crystals. *Acta Crystallogr.* **5**, 739–749 (1952)
68. J. Zhang, X. Shen, Y. Wang, C. Ji, Y. Zhou, J. Wang, F. Huang, X. Lu, Design of Two-Dimensional Multiferroics with Direct Polarization-Magnetization Coupling. *Phys. Rev. Lett.* **125**, 017601 (2020)
69. S.N. Ruddlesden, P. Popper, The compound Sr₃Ti₂O₇ and its structure. *Acta Crystallogr.* **11**, 54–55 (1958)
70. A.F. Wells, *Structural inorganic chemistry* (Clarendon, Oxford, 1984) p. 602
71. O. Yoon Seok, X. Luo, F.-T. Huang, Y. Wang, S.-W. Cheong, Experimental demonstration of hybrid improper ferroelectricity and the presence of abundant charged walls in (Ca,Sr)₃Ti₂O₇ crystals. *Nat. Mater.* **14**, 407 (2015)
72. B.H. Zhang, Z.Z. Hu, B.H. Chen, X.Q. Liua, X.M. Chen, Improved hybrid improper ferroelectricity in B-site substituted Ca₃Ti₂O₇ ceramics with a Ruddlesden–Popper structure. *J. Appl. Phys.* **128**, 054102 (2020)

73. S. Vasala, M. Karppinen, A2B'B''O6 perovskites: A review. *Prog. Solid State Chem.* **43**, 1–36 (2015)
74. T. Zhao, A. Scholl, F. Zavaliche, K. Lee, M. Barry, A. Doran, M.P. Cruz, Y.H. Chu, C. Eerer, N.A. Sapldin, R.R. Das, D.M. Kim, S.H. Baek, C.B. Eom, R. Ramesh, Electrical control of antiferromagnetic domains in multiferroic BiFeO₃ films at room temperature. *Nat. Mater.* **5**, 823–829 (2006)
75. H. Yang, L. Pan, M. Xiao, J. Fang, Y. Cui, Z. Wei, Iron-doping induced multiferroic in two-dimensional In₂Se₃. *Sci. China. Mater.* **63**, 421–428 (2020)
76. T. Song, X. Cai, M.W.-Y. Tu, X. Zhang, B. Huang, N.P. Wilson, K.L. Seyler, L. Zhu, T. Taniguchi, K. Watanabe, M.A. McGuire, D.H. Cobden, D. Xiao, W. Yao, X. Xu, Giant tunneling magnetoresistance in spin-filter van der Waals heterostructures. *Science* **360**, 1214–1218 (2018)
77. H. Wang, X. Qian, Two-dimensional multiferroics in monolayer group IV monochalcogenides. *2D Mater.*, **4**, 015042 (2017)
78. J. Qi, H. Wang, X. Chen, X. Qian, Two-dimensional multiferroic semiconductors with coexisting ferroelectricity and ferromagnetism. *Appl. Phys. Lett.* **113**, 043102 (2018)
79. C. Huang, Y. Du, H. Wu, H. Xiang, K. Deng, E. Kan, Prediction of intrinsic ferromagnetic ferroelectricity in a transition-metal halide monolayer. *Phys. Rev. Lett.* **120**, 147601 (2018)
80. X. Feng, J. Liu, X. Ma, M. Zhao, Ferroelectricity and multiferroicity in two-dimensional Sc₂P₂Se₆ and ScCrP₂Se₆ monolayers. *Phys. Chem. Chem. Phys.* **22**, 7489–7496 (2020)
81. Y. Lu, R. Fei, X. Lu, L. Zhu, L. Wang, L. Yang, Artificial multiferroics and enhanced magnetoelectric effect in van der Waals heterostructures. *ACS Appl. Mater. Interfaces* **12**, 6243–6249 (2020)
82. C. Gong, E.M. Kim, Y. Wang, G. Lee, X. Zhang, Multiferroicity in atomic van der Waals heterostructures. *Nat. Commun.* **10**, 2657 (2019)
83. Y. Su, X. Li, M. Zhu, J. Zhang, L. You, E.Y. Tsymlal, Van der Waals multiferroic tunnel junctions. *Nano Lett.* **21**, 175–181 (2021)
84. X. Li, J.T. Lü, J. Zhang, L. You, Y. Su, E.Y. Tsymlal, Spin-Dependent Transport in van der Waals Magnetic Tunnel Junctions with Fe₃GeTe₂ Electrodes. *Nano Lett.* **19**, 5133–5139 (2019)
85. K. Chang, J. Liu, H. Lin, N. Wang, K. Zhao, A. Zhang, F. Jin, Y. Zhong, X. Hu, W. Duan, Q. Zhang, L. Fu, Q.-K. Xue, X. Chen, S.-H. Ji, Discovery of robust in-plane ferroelectricity in atomic-thick SnTe. *Science* **353**, 274–278 (2016)
86. R. Fei, W. Kang, L. Yang, Ferroelectricity and phase transitions in monolayer group-IV monochalcogenides. *Phys. Rev. Lett.* **117**, 097601 (2016)
87. S.M. Poh, S.J.R. Tan, H. Wang, P. Song, I.H. Abidi, X. Zhao, J. Dan, J. Chen, Z. Luo, S.J. Pennycook, A.H. Castro Neto, K.P. Loh, Molecular-beam epitaxy of two-dimensional In₂Se₃ and its giant electroresistance switching in ferroresistive memory junction. *Nano Lett.* **18**, 6340–6346 (2018)
88. S. Wan, Y. Li, W. Li, X. Mao, W. Zhu, H. Zeng, Room-temperature ferroelectricity and a switchable diode effect in two-dimensional α -In₂Se₃ thin layers. *Nanoscale* **10**, 14885–14892 (2018)
89. F. Xue, W. Hu, K.-C. Lee, L.-S. Lu, J. Zhang, H.-L. Tang, A. Han, W.-T. Hsu, S. Tu, W.-H. Chang, C.-H. Lien, J.-H. He, Z. Zhang, L.-J. Li, X. Zhang, Room-temperature ferroelectricity in hexagonally layered α -In₂Se₃ nanoflakes down to the monolayer limit. *Adv. Funct. Mater.* **28**, 1803738 (2018)
90. L. You, F. Liu, H. Li, Y. Hu, S. Zhou, L. Chang, Y. Zhou, Q. Fu, G. Yuan, S. Dong, H.J. Fan, A. Gruverman, Z. Liu, J. Wang, In-plane ferroelectricity in thin flakes of van der Waals hybrid perovskite. *Adv. Mater.* **30**, 1803249 (2018)
91. T. Ghosh, M. Samanta, A. Vasdev, K. Dolui, J. Ghatak, T. Das, G. Sheet, K. Biswas, Ultrathin free-standing nanosheets of Bi₂O₂Se: Room temperature ferroelectricity in self-assembled charged layered heterostructure. *Nano Lett.* **19**, 5703–5709 (2019)
92. C. Xu, Y. Chen, X. Cai, A. Meingast, X. Guo, F. Wang, Z. Lin, T.W. Lo, C. Maunders, S. Lazar, N. Wang, D. Lei, Y. Chai, T. Zhai, X. Luo, Y. Zhu, Two-dimensional antiferroelectricity in nanostripe-ordered In₂Se₃. *Phys. Rev. Lett.* **125**, 047601 (2020)
93. M. Wu, X.C. Zeng, Intrinsic Ferroelasticity and/or multiferroicity in two-dimensional phosphorene and phosphorene analogues. *Nano Lett.* **16**, 3236–3241 (2016)
94. Y. Xu, C. Cheng, S. Du, J. Yang, B. Yu, J. Luo, et al., Contacts between two- and three-dimensional materials: Ohmic, Schottky, and p–n heterojunctions. *ACS Nano* **10**, 4895–4919 (2016)